Optical simulations for the laboratory-based expanded and collimated x-ray beam facility BEaTriX

D. Spiga, B. Salmaso, M. Bavdaz, C. Pelliciari, S. Basso, et al.

D. Spiga, B. Salmaso, M. Bavdaz, C. Pelliciari, S. Basso, V. Burwitz, I. Ferreira, M. Ghigo, E. Giro, G. Pareschi, M. Sanchez del Rio, G. Tagliaferri, G. Vecchi, E. Wille, "Optical simulations for the laboratory-based expanded and collimated x-ray beam facility BEaTriX," Proc. SPIE 11110, Advances in Laboratory-based X-Ray Sources, Optics, and Applications VII, 111100E (16 October 2019); doi: 10.1117/12.2530066

SPIE.

Event: SPIE Optical Engineering + Applications, 2019, San Diego, California, United States

Optical simulations for the laboratory-based, expanded and collimated X-ray beam facility BEaTriX

D. Spiga,[1*] B. Salmaso,[1] M. Bavdaz,[2] C. Pelliciari,[3] S. Basso,[1] V. Burwitz,[3] I. Ferreira,[2] M. Ghigo,[1] E. Giro,[1] G. Pareschi,[1] M. Sanchez del Rio,[4] G. Tagliaferri,[1] G. Vecchi[1], E. Wille[2]

[1]INAF – Brera Astronomical Observatory, Via Bianchi 46, 23807, Merate (Italy)
[2]European Space Agency, ESTEC, Keplerlaan 1, 2201 AZ Noordwjik, The Netherlands
[3]MPI für extraterrestrische Physik (MPE), Giessenbachstr., D-85748 Garching, Germany
[4]European Synchrotron Radiation Facility, 71, avenue des Martyrs, 38043 Grenoble, France

ABSTRACT

The construction of BEaTriX, the Beam Expander Testing X-ray facility, is underway at INAF-OAB (Osservatorio Astronomico di Brera). This laboratory-based X-ray source was designed to generate a broad (170 mm x 60 mm), uniform, and collimated X-ray beam, with a residual divergence of 1.5 arcsec HEW at either 1.49 keV and 4.51 keV. The main scientific driver for BEaTriX is represented by the opportunity to routinely calibrate the modular elements of the *ATHENA* (ESA) X-ray telescope, based on the silicon pore optics (SPO) technology. Nevertheless, the application domain of BEaTriX is potentially much wider (e.g., X-ray tomography). BEaTriX comprises a microfocus source of X-rays, followed by an optical chain including a collimating mirror, crystal monochromators, and an asymmetric beam expander. The final beam collimation and homogeneity relies on the optical quality of the optical components (X-ray source dimension, mirror polishing, crystal lattice regularity) and on their mutual alignment. In order to determine the most critical parameters, focus the development efforts, and establish specifications, a set of optical simulations has been built. Our paper describes the simulation tool we developed to this specific aim, and discusses the results achieved in terms of manufacturing and alignment tolerances.

Keywords: BEaTriX, X-ray test facility, micro-focus source, beam expander, optical simulation

1. INTRODUCTION

The pursuit of collimated (parallel) X-ray beams is probably as old as the discovery of X-rays. Unlike visible light, which can be easily made parallel by passing through a refractive lens, X-rays can be effectively handled only by diffraction or reflection. To this end, Fresnel lenses and parabolic mirrors are usually adopted, but these components require large ranges in high vacuum, for X-rays to propagate and be magnified to the required size. Consequently, not so many X-ray facilities worldwide are equipped to generate a collimated, broad, and intense X-ray beam. This poses a problem, chiefly in the domain of calibrations for astronomical X-ray optics, which are typically characterized by a large diameter and require a nearly-parallel X-ray beam to mimic the flux from a source at virtually infinite distance. For example, the PANTER X-ray facility at MPE, and the XRCF beamline at MSFC, represent reference points for the test and calibration of astronomical X-ray optics.

Nevertheless, large X-ray optics of future space telescopes will not be assembled from monolithic mirrors, and a very large number of their building blocks will have to be tested systematically to assess their focusing properties. The ATHENA X-ray telescope (Advanced Telescope for High-ENergy Astrophysics), the second large mission selected by ESA within the Cosmic Vision Program with launch scheduled in 2031, is progressing toward its realization. [1] It will be the largest X-ray telescope ever built, with a 2.4 m diameter a 1.4 m^2 effective area at 1 keV, and an angular resolution of 5 arcsec half-energy width (HEW). The optical assembly of ATHENA currently foresees 678 mirror modules (MM) based on the silicon pore optic (SPO) technology, which will be manufactured in series by Cosine, to be later [3] aligned and assembled, under UV light, into a bearing structure. Indeed, these mirror modules have to be systematically screened for optical quality and effective area at a foreseen production rate of 2 MM/day, before they can be integrated into the final ATHENA optic. The required screening pace, and the number of modules to be tested, would make large facilities unsuitable for that scope.

* e-mail: daniele.spiga@inaf.it - phone: +39-039-72320427

Advances in Laboratory-based X-Ray Sources, Optics, and Applications VII,
edited by Alex Murokh, Daniele Spiga, Proc. of SPIE Vol. 11110, 111100E
 · doi: 10.1117/12.2530066

Current tests of SPO modules [4] are performed in pencil-beam at the PTB lab at BESSY [5] or in full illumination at PANTER [6]. Tests of the complete ATHENA mirror can be performed at the VERT-X facility [7], currently supported by ESA and being designed by INAF-OAB (in collaboration with MediaLario, EIE group, and other Italian companies) via a raster scan of the ATHENA aperture with a small X-ray collimated beam. However, routine tests of SPOs at the required rate require a dedicated X-ray apparatus, able to generate a broad and nearly-parallel beam within a small lab size. To better understand how parallel the beam has to be, we have to remind that the individual MM for ATHENA cannot have a HEW exceeding 4.3 arcsec. Therefore, the beam used to fully illuminate the MM optical aperture should not diverge more than 2 arcsec. To that end, and given an upper limit of 11.6 cm for the MM lateral dimension, one should locate a point-like X-ray source at a 6 km distance under high vacuum. In order to avoid the need for such a large facility in SPO MM functional tests, we started in 2012 to design an X-ray facility [8] able to generate a broad (170×60 mm^2), uniform and low-divergent (1.5 arcsec HEW) X-ray beam within a small lab (~ 9×18 m^2). The design concept was based on the principle of vertical beam expansion via collimation on a paraboloidal mirror, spectral filtering at 4.5 keV, followed by horizontal beam expansion via asymmetric diffraction [9][10] on a silicon crystal. The facility design gradually evolved over time [11][12][13] toward the BEaTriX (the Beam Expander Testing X-ray facility) project [14][15], thanks to the AHEAD funding from EU H2020 and the current ESA support.

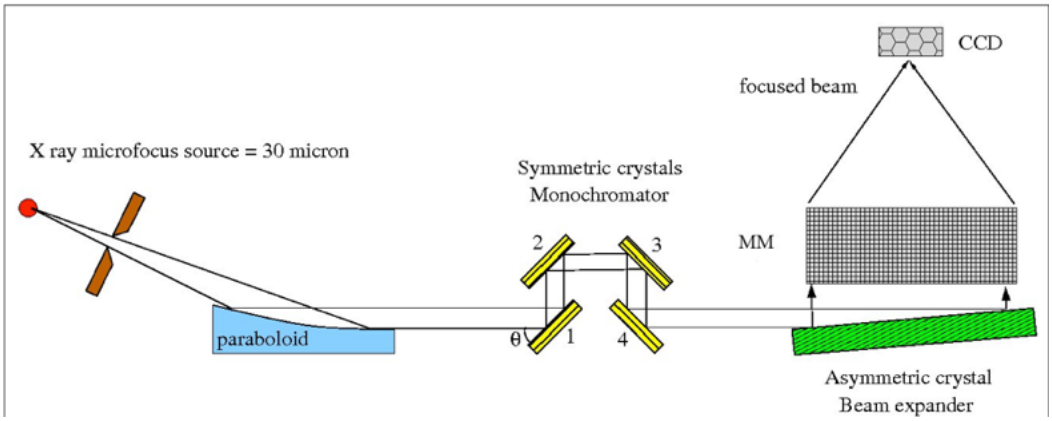

Figure 1: optical layout of the BEaTriX facility. Only the 4.51 keV beamline is shown. The parallel, polarized, and expanded X-ray beam has a final size of 170×60 mm^2 and a residual divergence of 1-2 arcsec. The beam is used to characterize the HEW and the effective area of an SPO mirror module.

BEaTriX consists of two beamlines (4.51 keV and 1.49 keV) in low vacuum (10^{-3} mbar) aiming at characterizing MMs at two significant energies in the ATHENA sensitivity band. The finalized design of the 4.51 keV beamline (Fig. 1) foresees the emission of X-rays from a microfocus (35 μm FWHM) source with Ti anode, in the focus of a paraboloidal mirror (f = 4750 mm) for collimation and vertical expansion to a 6 cm vertical size. [16] The source radiance is > 10^{11} ph/s/sterad in the Ti Kα doublet. The parallel beam is then spectrally filtered at the Kα1 line by two Si(220) channel cut crystals (CCC) in symmetric configuration. The first CCC is rotated by 12 arcsec, with respect to the ideal alignment, to improve the beam monochromation (Sect. 2.2). Finally, the expansion in the horizontal direction is achieved by another Si(220) crystal, this time asymmetrically cut at an angle of 45.6 deg. The expanded and parallel beam is used to illuminate the aperture of the mirror module, and the focal spot can be directly observed on a CCD camera, at a 12 m distance.

The 1.49 keV beamline will adopt a microfocus source in Ti-Al alloy, while the spectral filtering at 1.49 keV and the beam expansion will be performed replacing the silicon crystals with ammonium dihydrogen phosphate (ADP) ones. Preliminary ADP(101) samples have been already tested in X-rays, yielding very encouraging results. [17] Owing to the different Bragg and asymmetry cut angles, the expanded beams at either energy will have the same final direction when they impinge on the optical module under test. They will therefore share the same 12-m long vacuum tube to allow the beam propagation to the focal plane.

The BEaTriX construction is currently underway at INAF-OAB, and the beam line at 4.51 keV is expected to be completed by Q4 2020. A detailed description of the project and of the advancement status can be found in another SPIE volume [18]. In this paper, we briefly discuss the beam collimation requirement (Sect. 2) and provide detailed simulations of possible performance degradations caused by component misalignments (Sect. 3) or imperfections

(Sect. 4). Finally, we show how a wavefront sensor might be employed to diagnose the parabolic mirror misalignment (Sect. 5) and so assist the AIV (alignment, integration, and verification) process.

2. SYSTEM REQUIREMENTS AND SIMULATION CODE

2.1. Vertical collimation

As the beam monochromation, dispersion, collimation, and expansion effects occur only in the horizontal plane of BEaTriX, the beam divergence is expected to be different in the vertical and the horizontal directions. Since the SPO modules will have the incidence plane oriented vertically in BEaTriX, their optical quality will be tested to an accuracy that will mostly depend on the vertical divergence. Nevertheless, also the horizontal divergence is important to characterize a focal spot in two dimensions.

In the vertical direction, the beam divergence is mostly determined by source size and parabolic mirror misalignments. Imperfections of the parabolic mirror have little impact in the sagittal direction, due to the shallow incidence angle (0.9 deg). This makes the vertical divergence rather independent of the optical components in use and of the achieved monochromation. If the vertical collimation has to be better than 1.5 arcsec, and the paraboloid focal length is 4750 mm, we obtain that the HEW of the source cannot exceed 35 µm. For a symmetric 2D Gaussian source, the HEW exactly equals the FWHM. In reality, the vertical collimation is only affected by the source's vertical extent, which is a 1D Gaussian profile, so HEW ≈ 3/4 FWHM; therefore, with a 35 µm FWHM X-ray source we expect $HEW_{vert} \approx 1$ arcsec.

2.2. Horizontal collimation

The horizontal divergence is a more delicate point: it is affected by the source size, the mirror surface quality, the monochromator filtering capabilities, because asymmetric crystals are highly dispersive. In fact, each X-ray energy is diffracted at a different angle [9] according to the formula:

$$\cos\theta_2 - \cos\theta_1 = \frac{\lambda}{d}\sin\alpha \tag{1}$$

where $\alpha = 44.6$ deg is the asymmetry angle of beam expander, $d = 1.919$ Å is the d-spacing of the (220) diffraction order, $\theta_2 \approx 90$ deg, $\theta_1 \approx 1.2$ deg are the diffraction and the incidence angles respectively, and $\lambda \approx 2.75$ Å in the 4.51 keV setup. We obtain, differentiating,

$$\Delta\theta_2 = \frac{\sin\alpha}{d\ \sin\theta_2}\Delta\lambda + \frac{\sin\theta_1}{\sin\theta_2}\ \Delta\theta_1 \tag{2}$$

and we see that the second term is usually negligible, because the initial divergence $\Delta\theta_1$ is damped by the asymmetry factor (≈ 50). Therefore – provided that the X-ray source width and the mirror defects can be neglected - the final divergence is *mostly determined* by the passing bandwidth $\Delta\lambda$. Substituting the numbers in the first term, we get:

$$\Delta\theta_2 = \frac{\sin\alpha}{d\ \sin\theta_2}\Delta\lambda = \frac{0.71\ \lambda}{1.92\ \text{Å}}\frac{\Delta E}{E} = 46\,\Delta E\ \frac{\text{arcsec}}{\text{eV}} \tag{3}$$

In the absence of monochromation, the bandwidth is the one of the fluorescence line (≈ 1 eV) and would return a 46 arcsec horizontal divergence. In contrast, a 1.5 arcsec HEW in the final collimation requires $\Delta E < 0.03$ eV HEW. The bandwidth ΔE is primarily determined by the energy bandwidth of the monochromators $\Delta E_R = E \tan\theta_0\, \Delta\theta_R$, where $\Delta\theta_R = 6.5$ arcsec is the rocking curve HEW of Si (220) at 4.51084 keV, and $\theta_0 = 45.72$ deg is the incidence angle on the symmetric crystal. Another factor is represented by the angular dispersion of the beam $\Delta\theta_0$ before the monochromator, resulting from both source size and parabolic mirror quality. Assuming a convolution between the two contributions, we obtain for the energy bandwidth HEW,

$$\Delta E = E \tan\theta_0\ \sqrt{(\Delta\theta_R)^2 + (\Delta\theta_0)^2} \tag{4}$$

Thus, even taking a perfect mirror ($\Delta\theta_0 = 1$ arcsec, only due to the X-ray source size), Eq. 4 yields $\Delta E = 0.145$ eV, with a resulting divergence of 6.8 arcsec (Eq. 3). If $\Delta\theta_0 \approx 1.5$ arcsec because of the combined effect of source size and

mirror imperfections, the final divergence increases to 6.9 arcsec. We conclude that the limiting factor to the horizontal divergence is the width is monochromator's rocking curve width, $\Delta\theta_R$. Indeed, this parameter should be reduced to $\Delta\theta_R = 0.5$ arcsec to take the final beam divergence $\Delta\theta_2$ down to 1.5 arcsec or below. We can reduce $\Delta\theta_R$ implementing a monochromator design with four crystals (Fig. 1), clearly at the expense of the beam intensity. Nevertheless, the product of 4 identical rocking curves would certainly improve the peak-to tail ratio, but hardly return such a small bandpass, unless one or more crystals are tilted to de-tune the rocking curves. It has been already proven [14] that a double CCC system, with a CCC tilted by 12 arcsec, can satisfy this requirement and return a horizontal HEW = 1.5 arcsec. This will be re-simulated in detail and shown in Sect. 3.3 of this paper.

2.3. Flux intensity

The requirement on the beam flux stems from the need to characterize 3 MM/day, collecting 100000 focused counts per exposure in order to have a count statistics reliable within 0.3%. Considering the smallest mirror module with an approximate geometric area of 14 cm^2 and a reflectivity of 70% at 4.51 keV, we have an effective area of 7 cm^2 per module, and assuming to have approx. 30 min to integrate the flux, the beam density at the mirror module has to be $10^5/7$ $cm^2/1800$ s = 8 cts/s/cm^2. Summarizing, we have to reach a spectral filtering near 0.03 eV HEW and approx. 10 cts/s/cm^2 for the final beam density. The simulation code described in the next section aims at determining the configuration that enables both requirements.

2.4. BEaTriX modelling: IDL simulation code

The ray-tracing program we use to assess the system performance is the evolution of a previously-developed IDL code for BEaTriX [13]. We have made an extensive use of the code to determine the effects of the misalignments and the component imperfections. The ray-tracing code (Fig. 2) accounts for the properties of the optical components (reflectivity, acceptance, dispersivity, obstructions) and propagates the beam up to the mirror module location, where the expanded beam properties are analyzed.

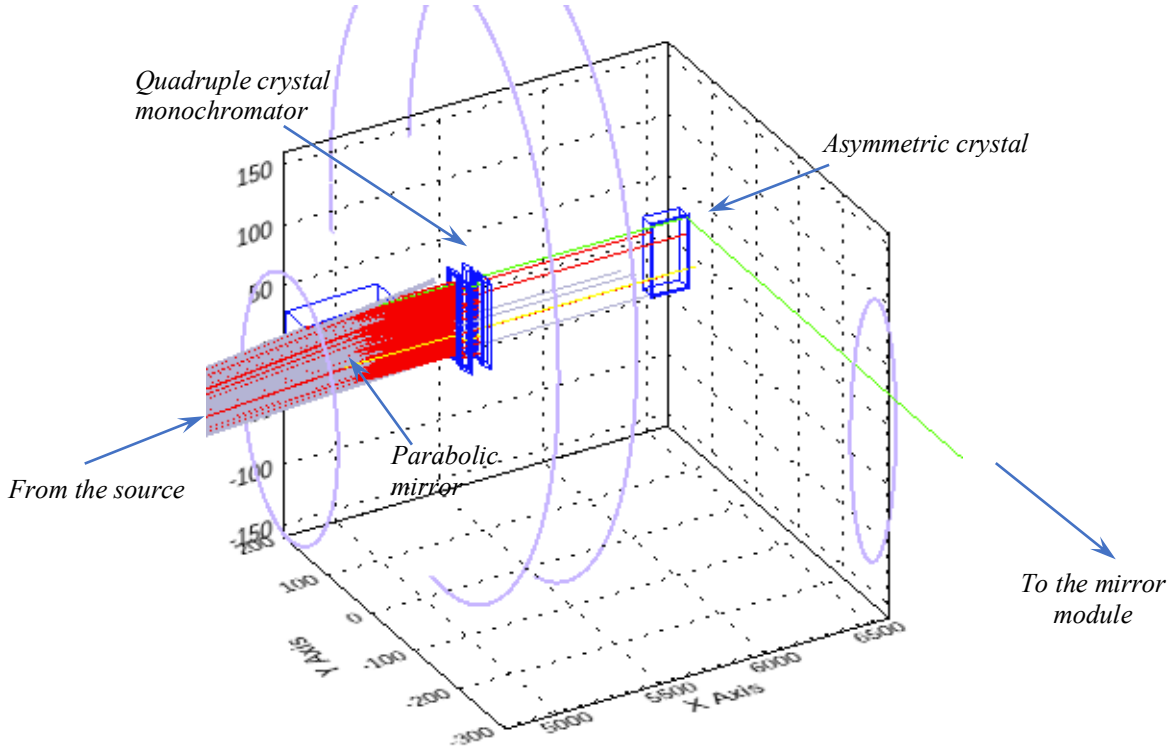

Figure 2: the reference frame used for the present description of the BEaTriX facility, and the components used to simulate the optical performances. Red rays are absorbed either in the reflection on the paraboloid, the crystals, or in the residual gas in the facility. Gray rays are blocked by diaphragms or non-optical surfaces. Yellow rays have missed the asymmetric crystal and have gone astray. Only a minority of rays (traced in green) are reflected by the asymmetric crystal and reach the mirror module.

All the simulation is performed in segments from element-to-element, rather than step-by step. This is possible because the ray intersection points with the optical elements are found analytically. The first few simulated rays are shown in Fig. 2. For practical reasons, the reference frame used in these simulations is different from the official frame of the BEaTriX project. [15] The simulation assumes as a starting point:

- A source radiance of 10^{11} ph/s/sterad from a Ti-anode source of 35 μm FWHM. The source radiance is the value integrated over the Ti-Kα doublet;
- Propagation in air, at a 10^{-3} mbar pressure;
- Reflection onto a Pt (30 nm) + C (4 nm) coated paraboloidal mirror at an average $\alpha = 0.9$ deg angle;
- Reflectivity of a Si (220) double CCC, slightly detuned (12 arcsec rotation) to narrow the passing band down to 0.03 eV;
- Reflectivity and dispersivity of a Si (220) crystal cut at an asymmetry angle of 45.6 deg.
- In the 1.49 keV setup, the Si crystals are replaced by ADP(101). However, the 1.49 keV line will not be implemented until the 4.51 keV line is completed, so we hereafter concentrate our analysis on the latter.

Running the simulation and launching an appropriate number of rays (> 10^6) we find that (as expected from the discussion in Sect. 2.2) at the system will meet the requirements of collimation (Figure 3): the vertical divergence HEW is less than 1 arcsec, and the horizontal divergence HEW is close to 1.5 arcsec. As for the expanded beam density at the MM under test (Figure 4), it is near 8 ph/s/cm^2, which makes it suitable for a full MM characterization (+- err. 0.3%) in a ½ h integration time.

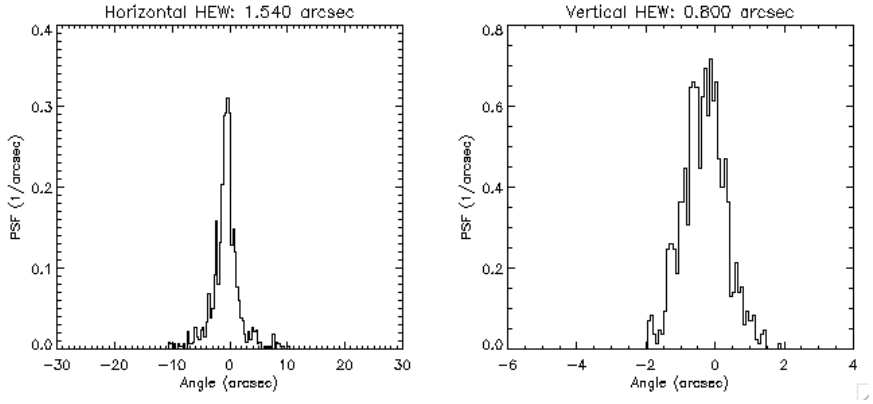

Figure 3: simulated performances in terms of (left) horizontal and (right) vertical beam divergence, assuming perfect components and alignment in the BEaTriX beamline at 4.51 keV.

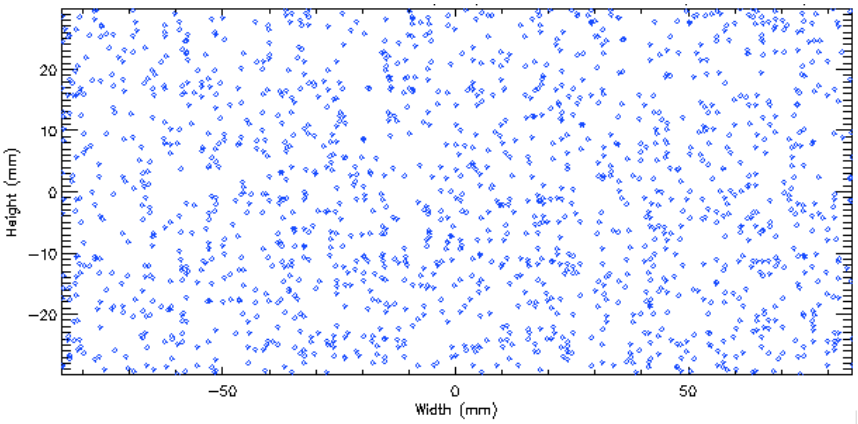

Figure 4: uniform distribution of rays at the location of the mirror module under test, over a 17 cm × 6 cm area, after launching 10^6 rays at energies within the Ti-Kα1 line width (0.8 eV). If the source has a radiance of 10^{11}ph/s/sterad in the Ti-Kα doublet, after re-normalization, the expected flux density will be 8 ph/s/cm^2. In reality, the X-ray source that will be purchased from Incoatec is expected to have a radiance >2 × 10^{11}ph/s/sterad in the same energy range.

In reality, the expected flux density at the MM comes from a conservative assumption on the source radiance of 10^{11} ph/s/sterad, and we performed all the simulations in this paper using this value. Nevertheless, the X-ray source has been recently tested, and we now know that we can rely on a source radiance at least twice as large. This would bring the achievable flux to > 16 ph/s/cm^2 at the MM entrance.

In the next section, we explore the effect of component misalignments on the system performances in terms of collimation and beam intensity.

3. MISALIGNMENT SIMULATIONS (4.51 KEV BEAMLINE)

3.1. Source displacements

Since the beam is parallel after the paraboloid, lateral translations of crystals are practically irrelevant. The only interesting case of positioning errors that can limit the BEaTriX performances is represented by the X-ray source displacement with respect to the paraboloid focus. Due to the long focal length of the mirror, this kind of misalignment is almost equivalent to a rotation of the parabolic mirror (Sect. 3.2). Both species of misalignments clearly generate aberrations in the collimated wavefront, which in turn causes inhomogeneity in the beam intensity and degrades the beam directionality. We show in Fig. 5 the beam distribution at the exit of the paraboloid when the source is centered in focus or displaced in either *y* or *z* direction. Besides the predictable effect of changing the beam direction in the opposite direction, the beam directionality is degraded orthogonally to the source displacement.

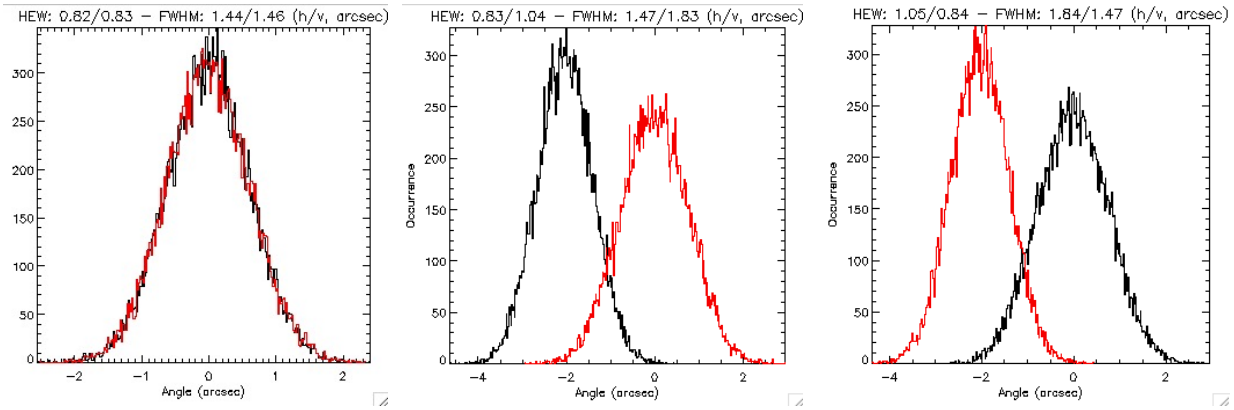

Figure 5: beam angular distribution after the reflection on the parabolic mirror. Left: source perfectly centered on-axis. Center: source displaced by -50 µm in y. Right: source displaced by +50 µm in z. Black line: horizontal distribution. Red line: vertical distribution. A source lateral displacement of 50 µm equals an angular deviation of 50 µm/(4750+436/2) mm = 2 arcsec.

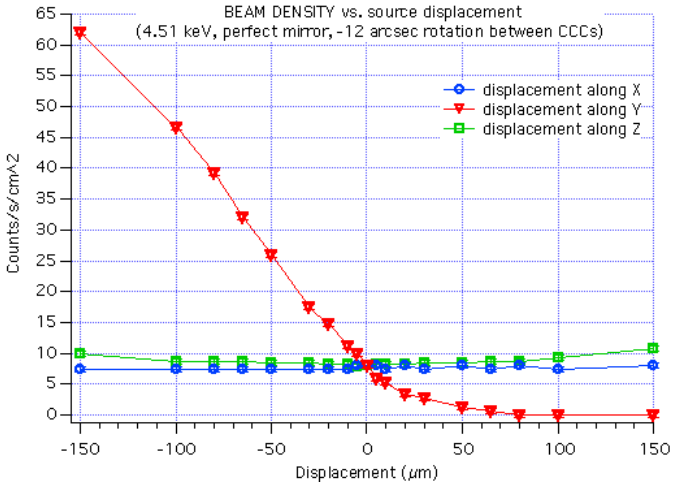

Figure 6: variation of beam intensity in BEaTriX, as a function of the X-ray source displacements along the 3 axes.

The source displacement effect on the beam intensity is shown in Figure 6. We note that:

1. The beam density is essentially unaffected by a movement Δx along the x-axis in the investigated range of ±0.15 mm (another displacement $-2\alpha\Delta x$ along y was added to keep the incidence angle constant).
2. In contrast, a displacement along y affects *heavily* the final intensity of the expanded beam. This is mostly due to the incidence angle variation on the monochromators: this moves the reflectivity of the first pair of crystals toward the peak ($\Delta y < 0$) or toward the tail ($\Delta y > 0$) of the rocking curve. In the former case, the source should not move along y by more than 10 µm. In the latter, even though a beam intensity increase is desirable, it would be paid with loss of monochromation and final horizontal divergence (Fig. 6). We can therefore set a limit of $|\Delta y| < 10$ µm in the source placing error.
3. Moving the source along the z-axis causes a very limited increase in the *average* beam density, caused by the spread in the exit angles in the horizontal plane, as shown in Fig. 5 right. It is noteworthy, however, that the deviation in the xy plane is quite small and closely correlated to the z coordinate on the mirror. The consequent variation with z of incidence angle on the monochromators affects the reflectivity in opposite directions. As a result, the vertical uniformity of the beam is expected to change with the vertical position of the X-ray source (Fig. 7). This effect can be useful to guide its alignment.

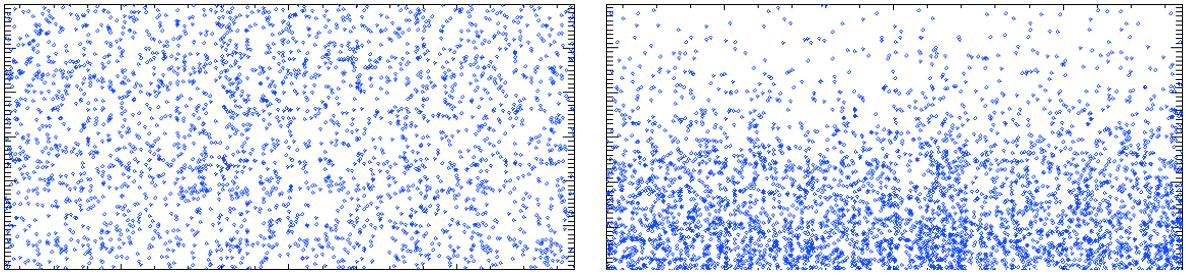

Figure 7: expanded beam uniformity (left) when the source is vertically aligned at z = 0 and (right) vertically misaligned at z = -150 µm. The full field is 170 mm × 60 mm.

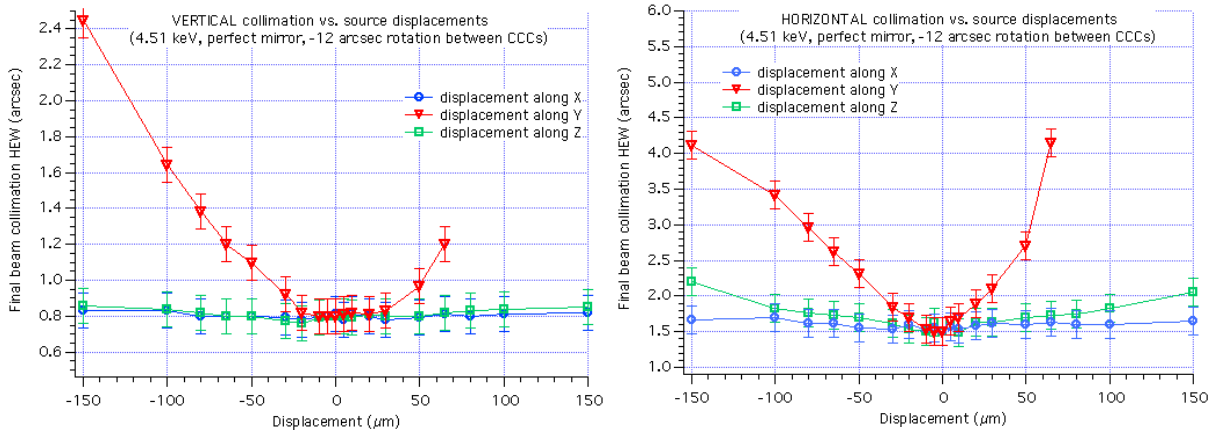

Figure 8: (left) vertical and (right) horizontal expected collimation of the BEaTriX expanded beam, as a function of the X-ray source displacements.

Regarding the beam collimation, the effect is markedly different for the three types of translations of the X-ray source. The vertical collimation (Fig. 8, left) is almost unaffected by displacements along x and z, with an HEW that does not exceed 1 arcsec in a quite wide range. The sensitivity to displacements in y is more pronounced, but the vertical HEW remains fairly constant within $|\Delta y| < 40$ µm. In all of these cases, the cause of the collimation degradation is only the off-axis aberration of the paraboloid.

The effect on the horizontal collimation is qualitatively similar (Fig. 8, right), even though the increase in collimation HEW stems this time from off-axis aberrations and horizontal beam steering, causing a less effective energy filtering in symmetric crystals. The horizontal HEW increases much more rapidly than it the vertical one, for both increasing displacements along y or z. Once again, it is the displacement along y that yields the dominant effect. Inspection of Fig. 8, right, shows that the source should stay still in its nominal position within $|\Delta y| < 10$ µm to avert

a relevant performance degradation, even if some correction is possible acting on the monochromators. Tolerances for Δz are much looser. Likewise, almost no impact on the HEW is detected in a 0.2 mm range of displacement along x.

3.2. Mirror rotations

An analogous effect to the X-ray source displacement can be simulated acting on the rotation of the parabolic mirror. Mirror translations are fully equivalent to translating the X-ray source, so we will not consider them here.

Mirror rotations (assumed to be about the center of the mirror's optical surface) have a similar effect to source translations, as far as wavefront aberrations are considered. Furthermore, due to the quite large focal length, even a small rotation will result in a large displacement of the focus. For example, a small rotation by $\Delta\theta_z$ about the z-axis moves the focus along y and is roughly equivalent to a displacement of the source by $\Delta y = -2f\Delta\theta_z$. Likewise, a rotation about the y-axis has almost the same effect as a source displacement by $\Delta z = -f\,\Delta\theta_y$; finally, a rotation about the x-axis simulates a source displacement $\Delta z = 2f\alpha\,\Delta\theta_x$. Due to the presence of the α factor, we expect that rotations about x will have negligible effect in a significant range (± 20 arcsec) of rotations around x. Conversely, a rotation about z exhibits the largest aberrations (Fig. 8) and it additionally steers the reflected beam by an angle twice as large as the equivalent source shift.

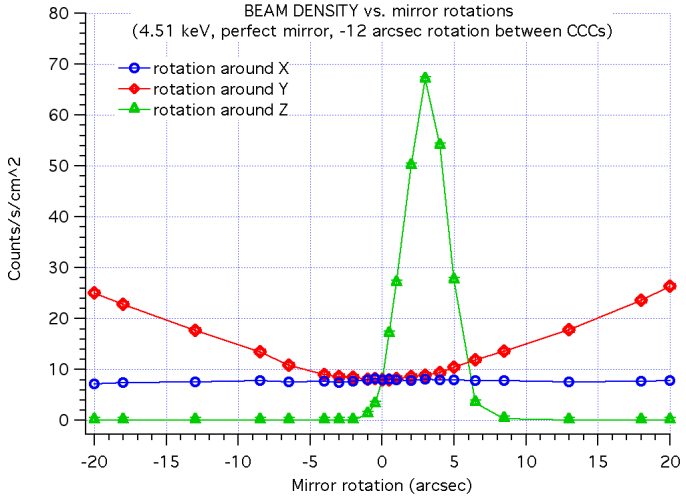

Figure 9: intensity of the BEaTriX expanded beam, as a function of the parabolic mirror rotations. To ease the comparison with Fig. 6, a 150 µm displacement along y is almost equivalent to a rotation around z of just -3.2 arcsec.

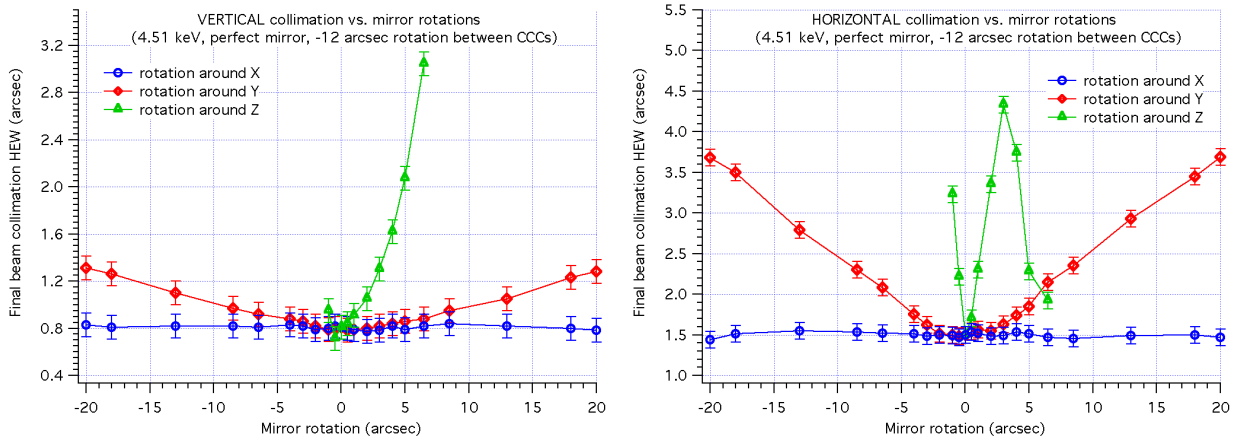

Figure 10: (left) vertical and (right) horizontal collimation of the BEaTriX expanded beam, as a function of the parabolic mirror rotations. To ease the comparison with Fig. 8, a 150 µm displacement along y is almost equivalent to a rotation around z of just -3.2 arcsec.

The simulated effect of the parabolic mirror rotations on the beam intensity is displayed in Fig. 9. The most prominent effect is the one of rotations about the *z*-axis (triangles). The reason is in the variation of the incidence angle on the symmetric crystals: the profile of the simulated curve reproduces the product of two CCC response, when they are mutually shifted by 12 arcsec. The much slower variation of the achievable flux with rotations around *y* are due to the angular beam spread in the horizontal plane (Fig. 5, right) causing a change of the incidence angle with *z*. An effect similar to Fig. 7, right, is observed with the beam uniformity. Finally, rotations around the *x*-axis are nearly irrelevant in the explored range of angles.

A totally similar behaviour can be simulated to assess the beam collimation in the vertical and horizontal planes (Fig. 10). The effect of the rotations about *z* seems to be the most pronounced one due to the change of incidence angles on the monochromators and the consequent broadening of the energy band impinging on the beam expander. In reality, this effect is correctable to a large extent by realigning the monochromators. On the other hand, a rotation around *z* causes aberrations in the vertical plane that cannot be corrected: at this regard, we can tolerate $|\Delta\theta_z| < 1$ arcsec without significantly degrading the vertical collimation. As for rotations about *y*, misalignments increase the horizontal divergence: they are, indeed, acceptable up to 2 arcsec.

3.3. Monochromator rotations

After the collimation operated by the parabola, the monochromation level is crucial in order to minimize the beam expander dispersivity (Sect. 2.2). We have already anticipated that the very narrow energy passband compatible with a 1.5 arcsec horizontal divergence can be obtained rotating the first CCC, with respect to the best superposition of the Bragg peaks. Figure 11 shows how this rotation affects the system performances. While a flux decrease by a 10-fold factor is expected, the collimation is improved by a factor of 3 (4.5 arcsec → 1.5 arcsec) if the two CCCs are de-tuned by a 12 arcsec, in either direction. The CCC rotation should be achieved to an accuracy of approx. 1 arcsec. The vertical divergence is not affected by the monochromation level.

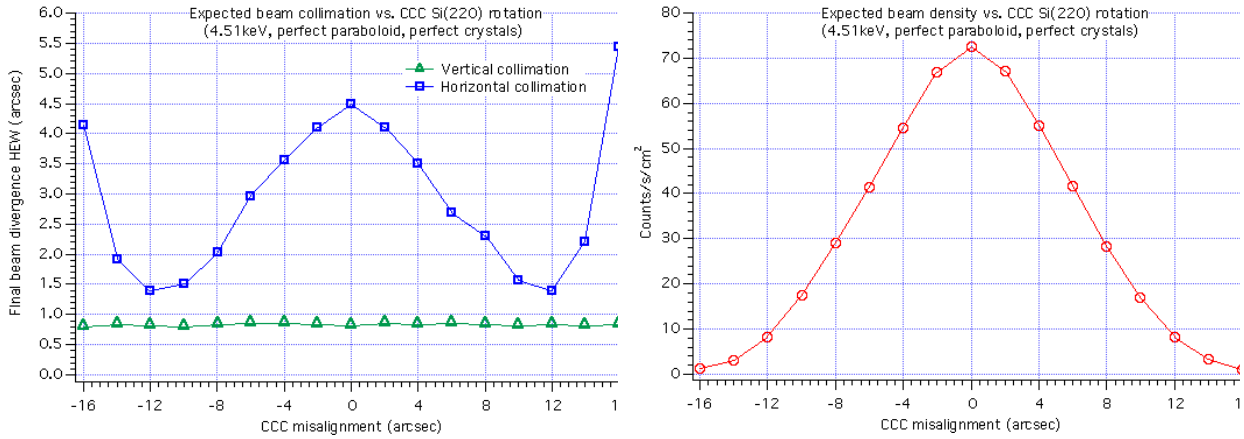

Figure 11: (left) collimation and (right) flux variation in the BEaTriX system at 4.51 keV using silicon monochromators, as a function of the angle between CCCs in Si(220), and a perfectly collimating mirror.

4. INTRODUCING COMPONENT IMPERFECTIONS

We have so far considered flawless components. However, we expect unavoidable manufacturing errors in the optical components for BEaTriX, which will clearly affect, to some extent, both the final flux intensity and the final collimation. As expected from the discussion in Sect. 2.2, the angular spread introduced by the mirror defects will broaden the energy bandpass. This turns into a larger angular spread after the asymmetric diffraction. As a result, both beam intensity and horizontal divergence increase with the mirror surface HEW. We have simulated this effect by imparting to the mirror profile the original map of the surface defects as received in a preliminary grinding and polishing status (HEW ≈ 60 arcsec). The profile has been damped by an appropriate factor in order to simulate an improving HEW value of the mirror, always keeping the nominal alignment of the CCCs. The simulation results are shown in Fig. 12: the flux increases with the square of the mirror HEW, and the final collimation is degraded linearly with the mirror HEW. The former is explained easily, because degrading the beam collimation increases the possible incidence-angle combinations and energy that fulfil the Bragg law within the rocking curve width of Si(220). For the

same reason, the energy band increases and the asymmetric crystal worsen the collimation in the horizontal direction (Fig. 12, right). As of today, the parabolic mirror has been improved to HEW ≈ 6 arcsec by the initial polishing process performed at OAB, which would return a horizontal divergence of about 3 arcsec in the expanded beam. We aim for a final optical quality of 0.5 arcsec, to be reached via super-polishing and ion beam figuring. [16]

The vertical collimation (Fig. 12, right) is mostly unaffected by the optical quality of the mirror, provided that azimuthal errors remain on the same order of magnitude of the longitudinal ones.

Figure 13 shows, finally, the effect of hypothetic mosaic structures in the silicon symmetric crystals. The rocking curves were degraded by convolution with Gaussian functions of increasing width. Even if mosaicity values up to 0.5 arcsec might be tolerated, we expect a nearly perfect crystalline structure in our silicon monochromators.

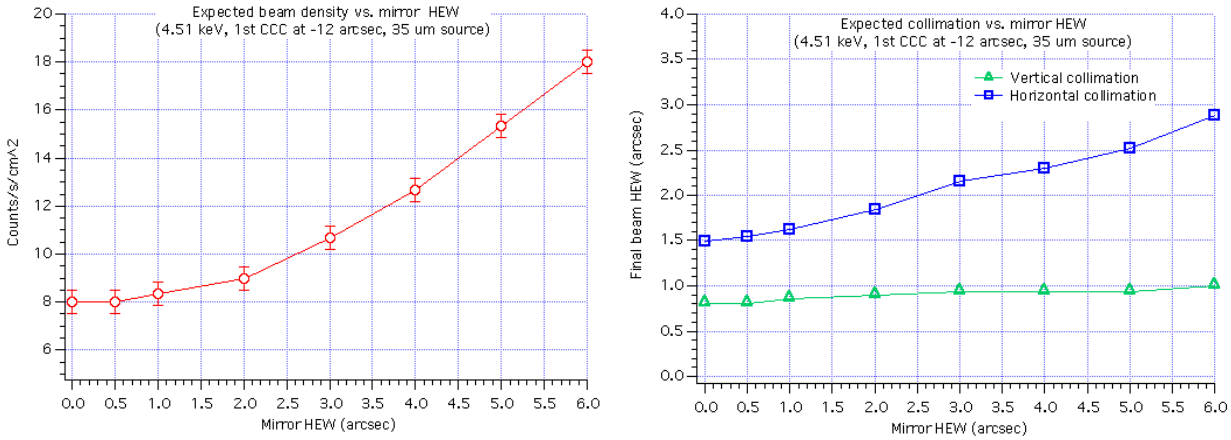

Figure 12: Left: final beam density variation with the parabolic mirror HEW. Right: final beam collimation degradation for increasing HEW values of the parabolic mirror.

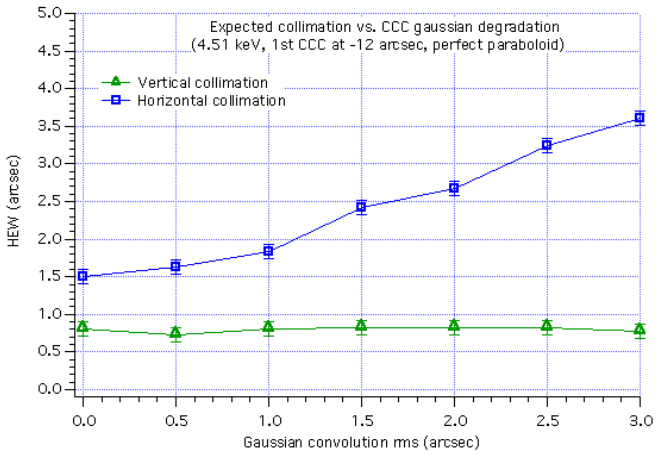

Figure 13: impact of crystalline imperfections, causing an increasing broadening of the Si(220) diffraction curves at 4.51 keV, on the final beam divergence.

5. DETECTING MISALIGNMENTS

We have now understood (Sect. 3) the effects of misalignments in BEaTriX, and the respective impacts on the imaging quality and the flux intensity. The problem now becomes how to recognize the different sources of misalignments and correct them during the AIV process. From the discussion in the previous sections, it should be quite clear that the most critical points are i) the alignment of the source to the focus of the parabolic mirror, and ii) the rotation of the monochromators with respect to the collimated beam at the exit of the parabola. Regarding i), our current AIV procedure foresees an initial alignment using a laser source, followed by a refinement by means of an X-ray Hartmann sensor. When the parabola is precisely aligned to the source, the beam is collimated and the monochromators can be used to filter the 4.51 keV line. Searching for the maximum flux after the CCC will allow us to locate the peak of Fig. 11, right, and subsequently narrow the passing band by rotating the first CCC by 12 arcsec. Finally, the asymmetric

crystal will be used to expand the beam: owing to the asymmetric geometry, [11] the alignment tolerances of the beam expander are quite loose, so the alignment of this components should not pose a problem. The final qualification of the beam will be performed by means of another Hartmann sensor.

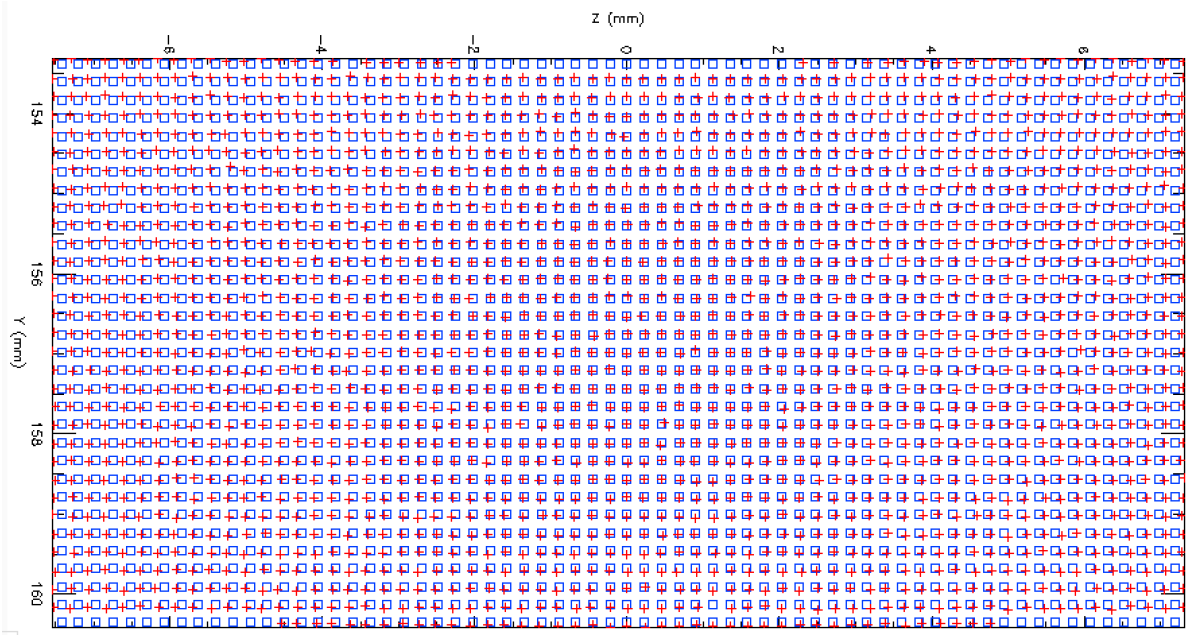

Figure 14: simulated output of a Hartmann sensor placed after the parabolic mirror (rotated by 90 deg). The blue squares represent the holes in the Hartmann plate. The crosshairs indicate the centroids of the beamlet emerging from each hole. The beam defocus, which can be clearly seen from the gradual decentering of the crosshairs from the plate center outwards, was deliberately exaggerated.

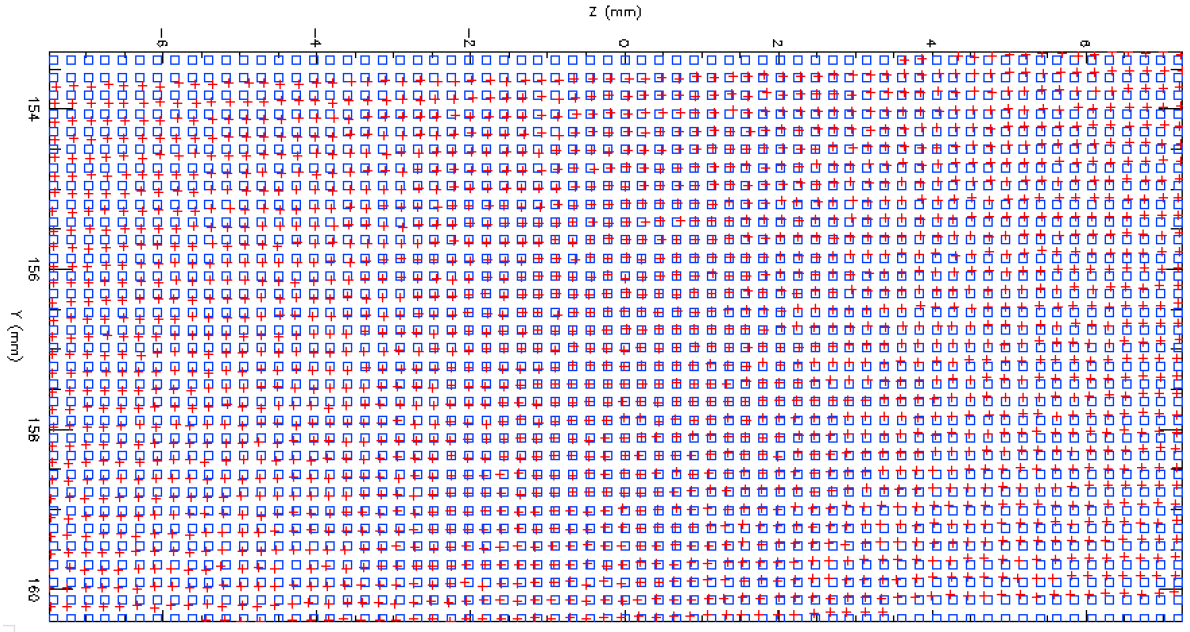

Figure 15: another simulated output of a Hartmann sensor placed after the parabolic mirror (rotated by 90 deg). In this case, we have simulated a large rotation of the paraboloidal mirror about the y-axis. The wavefront twist can be seen from the displacements of the crosshairs along the y-axis. This is exactly the effect that causes the beam intensity gradient in Fig. 7, right.

As for the interpretation of the wavefront sensor data during the alignment of the paraboloidal mirror, we already know that the observation of the flux gradient along the *z*-axis (Fig. 7) can be useful in order to detect the misalignment of the source along z (or, in an equivalent way, the rotation of the paraboloid around *y*). However, the most accurate detection of mirror misalignments comes from the wavefront analysis. As an example, we have simulated the output of a wavefront sensor with suitable characteristics, showing the expected displacement of the beamlets emerging from the Hartmann plate, as observed on the camera. For example, we have simulated in Fig. 14 a defocused X-ray source, and in Fig. 15 a rotation of the paraboloidal mirror around the *y*-axis. More generally, the displacements will be analyzed in terms of Zernike coefficients, [19] detecting and computing all the possible of misalignments listed in Sect. 3. This will provide us the information required to act on the respective motors and so correct the alignment.

6. CONCLUSIONS

In this paper, we have simulated the expanded beam of the BEaTriX X-ray facility in the 4.51 keV setup, being assembled in the INAF-OAB premises, showing that the required level of collimation (1.5 arcsec HEW) can be reached. We have analyzed some possible sources of errors, including misalignments and errors, that can limit the performances in the expanded beam intensity and collimation. All the requirements appear to be quite stringent, but achievable with the current equipment at OAB and with the motion systems that will be procured in the next months. Finally, we have started to simulate the expected outcome of a wavefront sensor that will be used to assist the source-mirror alignment in order to optimize the final performances at 4.51 keV. Future work will extend the simulations to the 1.49 keV beamline of BEaTriX.

ACKNOWLEDGMENTS

The development of the BEaTriX facility is funded by the ESA contract No. 4000123152/18/NL/BW, “Advanced and Compact X-ray Test facility for the ATHENA SPO module”, the AHEAD consortium activities financed by the EU Horizon 2020 grant No. 654215, and INAF internal funds.

REFERENCES

[1]. Bavdaz, M., Wille, E., Ayre, M., Ferreira, I., Shortt, B., et al., "Development of the ATHENA mirror," Proc. SPIE 10699, 106990X (2018)
[2]. Collon, M.J., Vacanti, G., Barrière, N., et al., “Status of the silicon pore optics technology,” Proc. SPIE 11119, 11110L (2019)
[3]. Valsecchi, G., Bianucci, G., Marioni, F., Zocchi, F.E., et al., “Integration facility for the ATHENA telescope,” Proc. SPIE 11119, 11110M (2019)
[4]. Vacanti, G., Barrière, N.M., Collon, M.J., Hauser, E., et al., "X-ray testing of Silicon Pore Optics," Proc. SPIE 11119, 1111901 (2019)
[5]. Krumrey, M., Muller, P. et al., "New X-ray parallel beam facility XPBF 2.0 for the characterization of the silicon pore optics," Proc. SPIE 9905, 99055N (2016)
[6]. Burwitz, V., Bavdaz, M, Wille, E., Collon, M., et al., “X-ray testing at PANTER of optics for the ATHENA and Arcus Missions,” Proc. SPIE 11180, 1118024 (2019)
[7]. Moretti, A., Pareschi, G., Uslenghi, M., Sironi G., Tordi, M., et al., “VERT-X: VERTical X-ray raster-scan facility for ATHENA calibration. The concept design,” Proc. SPIE 11119, 111190O (2019)
[8]. Spiga, D., Pareschi, G., Pelliciari, C., et al., “Functional tests of modular elements of segmented optics for x-ray telescopes via an expanded beam facility,” Proc. SPIE 8443, 84435F (2012)
[9]. Sanchez del Rio, M., Cerrina, F., “Asymmetrically cut crystals for synchrotron radiation monochromators”, Review of Scientific Instruments 63, 936 (1992)
[10]. Christensen, F., Hornstrup, A., Frederiksen, P., et al., "Expanded beam x-ray optics calibration facility at the Daresbury Synchrotron," Proc. SPIE 2011, 540 (1994)
[11]. Spiga, D., Pelliciari, C., Bonnini, E., et al., "An expanded x-ray beam facility (BEaTriX) to test the modular elements of the ATHENA optics," Proc. SPIE 9144, 91445I (2014)
[12]. Pelliciari, C., Spiga, D., Bonnini, E., et al., “BEaTriX, expanded soft x-ray beam facility for test of focusing optics, an update,” Proc. SPIE 9603, 96031P (2015)

[13]. Spiga, D., Pelliciari, C., Salmaso, B., et al. "Design and advancement status of the Beam Expander Testing X-ray facility (BEaTriX)," Proc. SPIE 9963, 996304 (2016)
[14]. Salmaso, B., Spiga, D., Basso. S., Ghigo, M., Giro, E., Pareschi, G., Tagliaferri, G., Vecchi, G., et al., "Progress in the realization of the beam expander testing x-ray facility (BEaTriX) for testing ATHENA's SPO modules," Proc. SPIE 10699, 1069931 (2018)
[15]. Salmaso, B., Spiga, D., Basso. S., Ghigo, M., Giro, E., Pareschi, G., Tagliaferri, G., Vecchi, et al., "BEaTriX (Beam Expander Testing X-ray facility) for testing ATHENA's SPO modules: advancement status," Proc. SPIE 11180, 1118026 (2019)
[16]. Vecchi, G., Salmaso, B., Basso, S., Sironi, G., et al., "BEaTriX, the Beam Expander Testing X-ray facility for testing ATHENA's SPO modules: the collimating mirror," Proc. SPIE 11119, 111191J (2019)
[17]. Ferrari, C., Beretta, S., Salmaso, B., Pareschi, G., Tagliaferri, G., et al., "Characterization of ADP crystals for soft x-ray optics of the Beam Expander Testing X-ray facility (BEaTriX)," Journal of Applied Crystallography 52, 599-604 (2019)
[18]. Salmaso, B., Basso, S., Giro, E., Spiga, D., Sironi, G., et al., "BEaTriX - the Beam Expander Testing X-ray facility for testing ATHENA's SPO modules: progress in the realization," Proc. SPIE 11119, 111190N (2019)
[19]. Cocco, D., Idir, M., Morton, D., Raimondi, L., Zangrando, M., "Advances in X-ray optics: From metrology characterization to wavefront sensing-based optimization of active optics," Nuclear Inst. and Methods in Physics Research A 907, 105-115 (2018)